AN IMPROVED ROUTINE FOR THE FAST ESTIMATE OF ION CYCLOTRON HEATING EFFICIENCY IN TOKAMAK PLASMAS

M. Brambilla

IPP 5/44 Februar 1992

MAX-PLANCK-INSTITUT FÜR PLASMAPHYSIK

8046 GARCHING BEI MÜNCHEN

MAX-PLANCK-INSTITUT FÜR PLASMAPHYSIK

GARCHING BEI MÜNCHEN

AN IMPROVED ROUTINE FOR THE FAST ESTIMATE OF ION CYCLOTRON HEATING EFFICIENCY IN TOKAMAK PLASMAS

M. Brambilla

IPP 5/44 Februar 1992

Die nachstehende Arbeit wurde im Rahmen des Vertrages zwischen dem Max-Planck-Institut für Plasmaphysik und der Europäischen Atomgemeinschaft über die Zusammenarbeit auf dem Gebiete der Plasmaphysik durchgeführt.

AN IMPROVED ROUTINE FOR THE FAST ESTIMATE OF ION CYCLOTRON HEATING EFFICIENCY IN TOKAMAK PLASMAS

M. Brambilla

ABSTRACT

The subroutine ICEVAL for the rapid simulation of Ion Cyclotron Heating in tokamak plasmas [1] is based on analytic estimates of the wave behaviour near resonances, and on drastic but reasonable simplifications of the real geometry. The subroutine has been rewritten to improve the model and to facilitate its use as input in transport codes. In the new version the influence of quasilinear minority heating on the damping efficiency is taken into account using the well-known Stix analytic approximation. Among other improvements are: a) the possibility of considering plasmas with more than two ion species; b) inclusion of Landau, Transit Time and collisional damping on the electrons non localised at resonances; c) better models for the antenna spectrum and for the construction of the power deposition profiles.

The results of ICEVAL are compared in detail with those of the full–wave code FELICE for the case of Hydrogen minority heating in a Deuterium plasma; except for details which depend on the excitation of global eigenmodes, agreement is excellent. ICEVAL is also used to investigate the enhancement of the absorption efficiency due to quasilinear heating of the minority ions. The effect is a strongly non–linear function of the available power, and decreases rapidly with increasing concentration. For parameters typical of Asdex Upgrade plasmas, about 4 MW are required to produce a significant increase of the single–pass absorpion at concentrations between 10 and 20 %.

1 – Introduction.

Numerical modeling of Ion Cyclotron heating of Tokamak plasmas has rapidly progressed in recent years. The computationally fastest approach is Ray Tracing [2], which however evaluates only the first transit absorption, it is accurate only in large devices, and cannot take into account the excitation of cavity eigenmodes. Next in sofistication are codes assuming a plane–layered geometry [3]: they provide accurate results for the loading resistance of the antenna and for the global repartition of the absorbed power between electrons and the different species of ions, but give at best qualitative information about power deposition profiles in tokamak geometry. The most advanced codes are fully toroidal [4], and provide both the global power balance and accurate power deposition profiles; on the other hand they are so slow that dedicated manpower is required to run even a single case completely. The need for a simpler and faster analysis is felt at least in two contexts: for a first shot–to–shot orientation during heating experiments, and to provide profiles of the h.f. power deposition for imput to transport codes. To satisfy these requirements, we have developed a fast subroutine ICEVAL [1] (Ion Cyclotron EVALuator), which estimates the power balance and the power deposition profiles during ICR heating of tokamaks using simple analytic estimates of the power spectre of the antenna and of the behaviour of the compressional wave near resonances.

The approach adopted in ICEVAL can be summarised as follows. In plasmas of sufficiently large dimensions a reasonable one–dimensional model of ICR heating can be constructed by retaining only the horizontal variation of density, temperature and magnetic field, while neglecting the poloidal magnetic field and the curvature of wavefronts (this is also the justification of full–wave codes in plane–layered geometry). In the same approximation moreover the wave behaviour near cyclotron and ion–ion hybrid resonances can be described sufficiently well by a straightforward generalisation of the classic Budden problem [5]. In this way the single–transit heating efficiency can be estimated, both globally and separately for each species of charged particles, without explicitly solving the wave equations. A simple algorithm can further be developed to obtain the total (multi–transit) power balance: it consists in the appropriate book–keeping of the power flowing in each direction in the regions between resonances, following each wave as it is transmitted and reflected at singular layers as long as needed to reach complete absorption. Damping by the electrons and losses at the walls can also easily be taken into account. A few adjustable parameters are provided which can be used to tune the results of ICEVAL on those of more sofisticated codes.

Reflection, transmission and absorption near each resonance depend critically on

the parallel wavenumber. For this reason it is necessary to regard the h.f. field as a superposition of toroidal modes, and to have an estimate of the fraction of the total power radiated by the antenna on each mode. A reasonable approximation to the radiated power spectrum can be obtained by weighting the toroidal Fourier spectrum of the antenna current with an exponential factor which takes into account evanescence in vacuum and in the plasma up to the R–cutoff. The algorithms which estimate the single transit and global power balances must be applied separately to each mode.

Once the global power balance is available, the evaluation of the radial power deposition profiles requires assumptions similar to those used for the same purpose in full–wave codes in slab geometry. Since resonance layers are quite narrow in the horizontal direction, the radial distribution of absorbed power is mainly determined by the unknown vertical distribution of incident power and absorption efficiency. On each resonance layer however by far the largest absorption occurs near the equatorial plane. A simple but plausible assumption for the vertical absorption pattern therefore allows a rough reconstruction of the radial power deposition profiles which is not too sensitive to the model used.

The equations used in ICEVAL are listed in the next section. In section 3 the algorithms needed to evaluate the first transit absorption, the global absorption and the power deposition profiles are presented. In section 4 we compare the results from ICEVAL with those obtained from a full-wave code in slab geometry for one of the most common IC heating scenarios. Some application of ICEVAL as a stand–alone package is also presented. Finally, the input and output variables of ICEVAL are listed in the Appendix.

Although perfect agreement of the very simple model used in ICEVAL with full–wave codes cannot be expected under all situations, those discrepancies which do occur are easily traced to the approximations made in each approach. In general, with some tuning of the adjustable parameters, the accuracy obtained with ICEVAL is comparable to that which can be expected from a full–wave code in slab geometry.

2 – Modelling IC heating.

In this section we summarise the equations used in ICEVAL, mostly without justification. Details can be easily found scattered in the literature on ICR heating, or can be worked out elementarily.

2.1 – The antenna spectrum. The power coupled by the antenna on each toroidal mode is estimated according to the following expression

$$P(n_\varphi) = P_o \, |J_A(n_\varphi)|^2 \, e^{-(\gamma_v + \gamma_p)} \, \tilde{f}(n_\varphi) \tag{1}$$

Here $J_A(n_\varphi)$ is the Fourier decomposition of the antenna current, the exponential factor takes into account evanescence in vacuum and in the plasma, and $\tilde{f}(n_\varphi)$ is a function which simulates the effects of the variation of the surface admittance of the plasma with $n_\parallel$ (the relation between the parallel index $n_\parallel$ and the toroidal wavenumber n_φ is $n_\parallel = n_\varphi/(k_o R_o)$, where R_o is the toroidal radius and $k_o = \omega/c$). Finally P_o is a constant which normalises the spectrum to the total power specified by the user.

Two options are available for the antenna configuration. In the case of a single conductor (often but rather unhappily referred to as the *monopole* antenna) we use

$$J_A(n_\varphi) = \frac{\sin(k_\parallel w_A/2)}{(k_\parallel w_A/2)} \tag{2}$$

where w_A is the width of the metallic strip (which is supposed oriented so that the current flows in the poloidal direction, as appropriate for excitation of the fast wave). In the case of two parallel conductors (similarly referred to as the *dipole* antenna) we use

$$J_A(n_\varphi) = \frac{\sin(k_\parallel w_A/2)}{(k_\parallel w_A/2)} \cos\left\{k_\parallel (w_A + g_A - \Phi_A)/2\right\} \tag{3}$$

where in the second factor g_A is the separation between the two conductors, and Φ_A the phase difference.

Evanescence in vacuum is given for $n_\parallel^2 > 1$ by

$$\gamma_v = 2k_o d_{ap} \sqrt{(n_\parallel^2 - 1)} \tag{4}$$

where d_{ap} is the distance between the antenna and the plasma surface. Similarly, evanescence in the plasma is estimated by

$$\gamma_p = 2k_o \int_a^{rco} |n_{\perp F}| \, dr \tag{5}$$

where the perpendicular index of the fast wave is given by the familiar approximation

$$n_{\perp F}^2 = -\frac{(n_\parallel^2 - R)(n_\parallel^2 - L)}{(n_\parallel^2 - S)} \tag{6}$$

and the integral extends from the plasma surface to the R–cutoff (the layer in which $n^2_{\perp F} < 0$). Both γ_v and γ_p are zero for $n^2_{\parallel} \leq 1$.

In the full antenna theory the evanescence factor is included in the surface admittance of the plasma, which moreover has a further weak dependence on $n_{\parallel}$. We simulate it in Eq. (1) with the function $\tilde{f}(n_\varphi)$. Empirically it has been found convenient to take

$$\tilde{f}(n_\varphi) = 1 + \hat{y}\frac{0.1n^2_{\parallel}}{1 + 0.1n^2_{\parallel}} \tag{7}$$

where $\hat{y}$ is a parameter which can be specified to improve similarity of the spectrum evaluated by (1) with the one from full–wave codes; the default value is 1. The value of $\hat{y}$ has no influence in the case of a dipole antenna; the factor $\tilde{f}$ is therefore taken to be unity in this case.

2.2 – Locating resonances and cut–offs. The first section of ICEVAL, after checking for the consistency of the input data, evaluates the position of cyclotron resonances of all ion species,

$$X(n, \alpha) = n\, R_o\, \frac{\Omega_{c\alpha}(R_o)}{\omega} \qquad\qquad (n = 1,\ 2) \tag{8}$$

where $\Omega_{c\alpha}(R_o)$ is the cyclotron frequency of species α at the toroidal radius (i.e. at the center of the vacuum chamber) and $X(n, \alpha)$ is measured from the vertical axis. Fundamental resonances $X(1, \alpha)$ and first harmonic resonances $X(2, \alpha)$ not coinciding with a fundamental resonance of another species are then sorted in order of decreasing distance from the vertical axis, discarding those which lie outside the plasma. The equatorial plasma cross–section is thereby divided in a number of regions, separated by the cyclotron resonances layers.

For each fundamental cyclotron resonance within the plasma not belonging to the "majority" species, the position of the associated ion–ion hybrid cutoff and resonance,

$$X_{cof}(m) = H_{cof} \cdot X(1, m) \qquad\qquad X_{res}(m) = H_{res} \cdot X(1, m) \tag{9}$$

are then determined. If only two ion species are present, explicit formulae are available for H_{cof} and H_{res}, namely

$$H_{cof} = 1 + \nu_m Z_m \left\{ \frac{Z_M/A_M}{Z_m/A_m} - 1 \right\}$$

$$H_{res} = \left\{ \frac{1 + \nu_m Z_m \left(\dfrac{Z_M/A_M}{Z_m/A_m} - 1 \right)}{1 + \nu_m Z_m \left(\dfrac{Z_m/A_m}{Z_M/A_M} - 1 \right)} \right\}^{1/2} \tag{10}$$

where subscripts M and m refer to the "majority" and "minority" species, respectively; the charge Z and mass A of each species are in atomic units (i.e. $A = Z = 1$ for protons), and $\nu_\alpha = n_\alpha/n_e$ is the number concentration of species α.

If more than two ion species are present, H_{cof} and H_{res} are obtained iteratively from

$$H_{cof} = 1 + \frac{\nu_m Z_m}{Q_{cof}} \qquad H_{res} = \left\{1 + \frac{\nu_m Z_m}{Q_{res}}\right\}^{1/2} \tag{11}$$

where Q_{cof} and Q_{res}, which depend weakly on H_{cof} and H_{res},

$$\begin{aligned} Q_{cof} &= \sum_{i \neq m} \nu_i Z_i \frac{Z_m/A_m}{(Z_i/A_i) - H_{cof}(Z_m/A_m)} \\ Q_{res} &= \sum_{i \neq m} \nu_i Z_i \frac{(Z_m/A_m)(Z_i/A_i)}{(Z_i/A_i)^2 - H_{res}^2(Z_m/A_m)^2} \end{aligned} \tag{12}$$

are evaluated the first time with $H_{cof} = H_{res} = 1$.

Isolated first harmonic resonances are also associated with a cutoff and a confluence (with the lowest Bernstein wave), and are essentially similar to ion–ion hybrid resonances. The corresponding positions are again given by (9) with

$$\begin{aligned} H_{cof} &= 1 - (2 - \sqrt{3})\frac{\beta_M}{2} \simeq 1 - 0.13\beta_M \\ H_{res} &= 1 - (2 - \sqrt{3})\frac{\beta_M}{2} \simeq 1 - 1.86\beta_M \end{aligned} \tag{13}$$

(both points are to the high field side of the harmonic).

When the first harmonic of one species coincides with the fundamental resonance of another (the situation for H^+ minority in a D^+ plasma), Eqs. (10) and (12) should be modified by a correcture of order $\sqrt{\beta/\nu_m}$; in practice this correcture can be neglected as soon as $\nu_m \gg \beta$ (however, the corresponding contribution to the *optical thickness* of the evanescence layer between cut–off and resonance is taken into account, cfr. the next subsection).

The majority species M has to be identified by the user. Although it is not necessary that $\nu_i Z_i \ll \nu_M Z_M$ for all $i \neq M$, it is clearly convenient that the fundamental cyclotron resonance of species M should not lie within the plasma. The presence of first harmonic of the majority on the other hand makes no problem.

2.3 – Mode conversion. The behaviour of a wave incident on an ion–ion hybrid resonance is essentially described by the classical Budden model. The corresponding optical thickness is in the case of an isolated resonance

$$\eta_1 = \kappa_1 \frac{\pi}{2} n_{\perp F} k_o |X_{cof} - Xres| \tag{14}$$

and in the case of pure first harmonic heating

$$\eta_2 = \kappa_2 \frac{\pi}{16} n_{\perp F} k_o R_c \cdot \left(\frac{n_\parallel^2 - \mathcal{R}_o}{n_\parallel^2 - \mathcal{S}_o} \right)^2 \beta_i \tag{15}$$

where the cold dielectric tensor elements and $n_{\perp F}$ have to be evaluated neglecting the contribution of the resonant species m:

$$\mathcal{R}_o = \sum_{i \neq m} \frac{\omega_{pi}^2}{\Omega_{ci}^2} \frac{1}{1+h_i} \qquad \mathcal{L}_o = \sum_{i \neq m} \frac{\omega_{pi}^2}{\Omega_{ci}^2} \frac{1}{1-h_i} \tag{16}$$
$$\mathcal{S}_o = \frac{1}{2}(\mathcal{R}_o + \mathcal{L}_o)$$

with $h_i = \omega/\Omega_{ci}$ at $R = R_c$, and

$$n_{\perp F}^2 = -\frac{(n_\parallel^2 - \mathcal{L}_o)(n_\parallel^2 - \mathcal{R}_o)}{(n_\parallel^2 - \mathcal{S}_o)} \tag{17}$$

Finally, κ_1 and κ_2 are numerical factors which should take into account that wavefronts are not strictly vertical ($\kappa_i \geq 1$, where the lower limit applies to vertical wavefronts; in practice, the κ_i's can be adjusted by the user to match for example the results of ray tracing).

The wave equations in the case of a degenerate resonance (H^+ in D^+) have not been solved analytically. It is nevertheless clear that the total optical thickness η must have η_1 as limit for $\nu_m \gg \beta_M$, and η_2 as limit for $\nu_m \to 0$. We assume the correct transition formula between these two limits to be

$$\eta = \eta_1 + \sqrt{\eta_2 (\eta_1 + \eta_2)} \tag{18}$$

This is suggested by analogy with the dependence of the physical thickness of the evanescence layer on β_M and ν_m; the non–analytic behaviour of η in the limit $\beta_M \to 0$ would also explain the intractability of the wave equation when β_M and ν_m are of the same order.

The coefficients of power reflection, transmission and wave conversion through the ion–ion resonance–cutoff layer are given in terms of η as follows:
a) wave incident from the low magnetic field side:

$$R_+ = (1 - e^{-2\eta})^2 \qquad T_+ = e^{-2\eta} \qquad A_+ = e^{-2\eta}(1 - e^{-2\eta}) \tag{19}$$

b) wave incident from the high magnetic field side:

$$R_- = 0 \qquad T_- = e^{-2\eta} \qquad A_- = 1 - e^{-2\eta} \tag{20}$$

Here $A_\pm$ is the fraction of incident power which is mode–converted into the Bernstein branch; it is assumed that this power is totally absorbed near the conversion layer. If the Bernstein wave propagates *away* from the cyclotron resonance (minority lighter, i.e. with larger charge to mass ratio, than majority) it is attributed totally to the electrons. In the opposite case (minority heavier, i.e. with smaller charge to mass ratio, than majority) it is attributed to the electrons if $\omega/k_\parallel v_{the} \leq 2.5$, to the minority ions in the opposite case.

2.4 – Direct ion cyclotron damping. Direct ion cyclotron damping of the fast wave by minority ions can be estimated by taking the spatial variation of the electric field from the solution of the Budden wave equation, and integrating the power balance equation through the Doppler–broadened cyclotron layer. The parameter

$$\epsilon_c = \frac{1}{2} n_\parallel^2 \frac{v_{thm}^2}{c^2} \left(\frac{R_m}{X_{res} - R_m} \right)^2 \tag{21}$$

determines wether damping takes place in the *minority regime* ($\epsilon_c \gg 1$), in which screening of the left–handed field E_+ by the resonant ions is negligible, or in the *mode conversion regime* ($\epsilon_c \ll 1$), in which screening of E_+ is strong. Both regimes are covered by writing the fractional power absorption of the fast wave by the minority ions as

$$\alpha_m^1 = \pi \frac{\epsilon_c}{1 + \epsilon_c} \frac{\omega_{pm}^2}{\Omega_{cm}^2} \left| \frac{(n_\parallel^2 - \mathcal{R}_o)}{(n_\parallel^2 - \mathcal{L}_o)(n_\parallel^2 - \mathcal{S}_o)} \right| (k_{\perp F} R_m) \tag{22}$$

where $k_{\perp F} = k_o n_{\perp F}$. Similarly, first harmonic damping by species j gives a fractional absorption

$$\alpha_j^2 = \frac{\pi}{4} \beta_j \left| \frac{(n_\parallel^2 - \mathcal{R}_o)}{(n_\parallel^2 - \mathcal{L}_o)(n_\parallel^2 - \mathcal{S}_o)} \right| (k_{\perp F} R_m) \tag{23}$$

Near an isolated ion–ion resonance α_j^2 is of course absent.

Note that Eqs. (21) and (22) describe damping of the fast wave, while $A_{\pm}$ in Eqs. (19) describe damping of the mode–converted wave. In this simple model the two processes are assumed to be additive; this might lead to overestimate somewhat absorption in the minority regime. Numerical solutions of the wave equations show that mode conversion is strongly suppressed as soon as appreciable cyclotron damping occurs near the mode conversion layer. To take this into account, we have modified the expressions for the optical thickness with a factor which becomes small when the Doppler width of the cyclotron resonance overlaps with the ion–ion resonance:

$$\eta_{eff} = \frac{\eta}{1 + 10.\, Q_{doppl}\, \epsilon_c} \tag{24}$$

The parameter Q_{doppl} is available to the user: putting it equal to unity means that suppression of mode conversion begins when $|\omega - \Omega_{cm}| \simeq 3 k_{\parallel} v_{thm}$, which seems appropriate for isolated ion–ion resonances.

2.5 – Stix corrections to the minority temperature. Estimates of the effective temperature reached by minority ions have been obtained by Stix [6]. In their simplest form, they can be written

$$T_{m,eff} = \frac{3\sqrt{\pi}}{4} Z_m \frac{v_{the}}{v_{thm}}\, D_{QL} \tag{25}$$

where D_{QL} is the normalised quasilinear diffusion coefficient. D_{QL} in turn can be written in terms of the heating rate W_m and the concentration ν_m of the minority ions as

$$D_{QL} \simeq 3.5\, 10^{-3} \frac{Z_m Z_M}{A_m A_M} \frac{T_M^{1/2}}{(10^{-14} n_e)^2\, \nu_m} W_m \tag{26}$$

(T_M in keV, W_m in Watt/cm^3).

Since the heating rate is not known in advance, the corrections due to the increased effective temperature of the minority ions must be evaluated iteratively. The total power P_m deposited in the minority in the ohmic plasma is used for a first guess to estimate the effective minority temperature; the power balance is then reevaluated using the corrected temperature, and so on. This procedure converges in two or three iterations. Unfortunately, a rather large uncertainty arises in relating the heating rate W_m to the available power P_m,

$$W_m = \frac{P_m}{\Delta V_{eff}} \tag{27}$$

since the effective volume in which heating occurs is badly defined. To estimate ΔV_{eff} we have made assumptions similar to those described below for the evaluation of the power deposition profiles:

$$\Delta V_{eff} = 2\pi^2 R_o r_m \, \Delta r \qquad\qquad \Delta r = \sqrt{h^2 + r_m^2} - r_m \tag{28}$$

where r_m is the minor radius at the cyclotron resonance of the minority ions, and h the effective vertical height of the illuminated zone (cfr.section 3.3).

It should also be noted that Eqs. (25)–(26) are likely to overestimate somewhat quasilinear effects on the efficiency of cyclotron damping by the minority species. In the first place, these equations assume that the minority distribution function remains isotropic; in reality, the ions gain mainly perpendicular energy, while damping depends mainly on the parallel temperature. A simple estimate of the degree of temperature anysotropy which is actually allowed by collisions is not available. Even more important however is the fact that a careful inspection of Stix derivation shows that only a fraction (typically between 10 and 50 %) of the minority ions are in the tail with the effective temperature given by Eq. (25).

In view of the large uncertainty in ΔV_{eff} we have not attempted to improve analytically the estimates (25)–(26); instead, a free coefficient κ_{QL} is included in the definition of D_{QL} (with default value $\kappa_{QL} = 1$), which can be used to tune the results on those obtained with combined Fokker–Planck and full–wave codes, if available.

2.6 – Electron damping and losses at the walls. Provided $\beta_e \gtrsim m_e/m_i$, the fractional power absorption for the fast wave due to the combined effect of TTMP and Landau damping by the electrons in the layer between two resonances at $R = X_1$, $R = X_2$, can be estimated from

$$\alpha_{TTe} = 1 - e^{-2k_o \int_{X_1}^{X_2} \gamma_e(R) dR} \tag{29}$$

where γ_e is given as a function of density and temperature by

$$\gamma_e = \sqrt{\pi}\, n_{\perp F} \frac{\omega_{pe}^2}{\Omega_{ce}^2} \frac{v_{the}^2}{c^2}\, x_{0e} e^{-x_{0e}^2} \tag{30}$$

with $x_3 = \omega/k_\parallel v_{the}$. The integral is evaluated as a simple sum over plasma layers of the radial mesh of the power deposition profiles (section 3.3).

At low temperatures, a significant amount of collisional damping in the outer plasma layers is predicted by full–wave codes [3], particularly if absorption by other mechanisms

is weak. This gives an additional contribution to γ_e of the form

$$\gamma_e^{coll} \simeq \frac{1}{n_{\perp F}} \frac{\omega_{pe}^2}{\Omega_{ce}^2} \frac{2\nu_c}{\Omega_{ce}} \qquad \text{with } \nu_c = 2.8\,10^{-9} \frac{n_e}{T_e^{3/2}} \tag{31}$$

(n_e in cm^{-3}, T_e in keV; only the dominant contribution from the $\vec{E} \times \vec{B}$ drift of the electrons is taken into account).

Finally, as a plane wave is reflected by a wall, a fraction α_w of its power flux is assumed to be lost. This can simulate any parasitic loss such as radiation through the vessel apertures, excitation of parametric instabilities, nonlinear sheath rectification near the Faraday screen, etc.. For the purpose, the values α_w^e and α_w^i at the outer and inner wall can be chosen independently.

3 – Power balance and power deposition profiles.

We now illustrate how the previous equations are used in ICEVAL to obtain the global power balance. The assumptions made to estimate the power distribution profiles are then presented in the second part of the section.

3.1 – Power balance near a resonance layer. The equations of the previous section immediately allow a power balance analysis of a transit through a resonance layer $X = X^{(k)}$. Let

$\alpha_e^{(k)} =$ Fraction of power damped to the electrons between $X^{(k-1)}$ and $X^{(k)}$

$\alpha_m^{(k)} =$ Fraction of power damped to the minority ions near $X^{(k)}$

$\alpha_M^{(k)} =$ Fraction of power damped to the majority ions near $X^{(k)}$

$\tau_e^{(k)} = 1 - \alpha_e^{(k)}$

$\tau_i^{(k)} = 1 - (\alpha_m^{(k)} + \alpha_M^{(k)})$

$A_\pm^{(k)} =$ Mode conversion efficiency near $X^{(k)}$

$R_\pm^{(k)} =$ Reflection coefficient from $X^{(k)}$

$T_\pm^{(k)} =$ Transmission coefficient from $X^{(k)}$

where suffixes $+$, $-$ apply to waves moving towards and away from the vertical axis, respectively. For each of these quantities an explicit expression was given in the previous section.

Depending on the relative positions of cyclotron and wave resonances and on the incidence side of the wave, the fraction of incident power which flows into the different available channels as a wavefront transits through $X^{(k)}$ will be as follows:

1 a) Wave incident from the low magnetic field side, minority cyclotron resonance to the outside of the ion–ion resonance:

- to the electrons	$\alpha_e^{(k)} + \tau_e^{(k)}\,\tau_i^{(k)}\,A_+^{(k)}\,\gamma_e^{(k)}$
- to the minority ions	$\tau_e^{(k)}\left\{\alpha_m^{(k)} + \tau_i^{(k)}\left(R_+^{(k)}\alpha_m^{(k)} + A_+^{(k)}\gamma_i^{(k)}\right)\right\}$
- to the majority ions	$\tau_e^{(k)}\left(\alpha_M^{(k)} + \tau_i^{(k)} R_+^{(k)}\alpha_M^{(k)}\right)$
- reflected	$\tau_e^{(k)}\tau_i^{(k)} R_+^{(k)}\tau_i^{(k)}$
- transmitted	$\tau_e^{(k)}\tau_i^{(k)}T_+^{(k)}$

1 b) Wave incident from the low magnetic field side, minority cyclotron resonance to the inside of the ion–ion resonance:

- to the electrons	$\alpha_e^{(k)} + \tau_e^{(k)}\,A_+^{(k)}\,\gamma_e^{(k)}$
- to the minority ions	$\tau_e^{(k)}\left(A_+^{(k)}\gamma_i^{(k)} + T_+^{(k)}\alpha_m^{(k)}\right)$
- to the majority ions	$\tau_e^{(k)}\,\alpha_M^{(k)}\,T_+^{(k)}$
- reflected	$\tau_e^{(k)}\,R_+^{(k)}$
- transmitted	$\tau_e^{(k)}\tau_i^{(k)}T_+^{(k)}$

2 a) Wave incident from the high magnetic field side, minority cyclotron resonance to the outside of the ion–ion resonance:

- to the electrons	$\alpha_e^{(k+1)} + \tau_e^{(k+1)}\,A_-^{(k)}\,\gamma_e^{(k)}$
- to the minority ions	$\tau_e^{(k+1)}\left(A_-^{(k)}\gamma_i^{(k)} + T_-^{(k)}\alpha_m^{(k)}\right)$
- to the majority ions	$\tau_e^{(k+1)}\,\alpha_M^{(k)}\,T_-^{(k)}$
- reflected	$\tau_e^{(k+1)}\,R_-^{(k)}$
- transmitted	$\tau_e^{(k+1)}\tau_i^{(k)}T_-^{(k)}$

2 b) Wave incident from the high magnetic field side, minority cyclotron resonance

to the inside of the ion–ion resonance:

- to the electrons	$\alpha_e^{(k+1)} + \tau_e^{(k+1)}\,\tau_i^{(k)}\,A_-^{(k)}\,\gamma_e^{(k)}$
- to the minority ions	$\tau_e^{(k+1)}\left\{\alpha_m^{(k)} + \tau_i^{(k)}\left(R_-^{(k)}\alpha_m^{(k)} + A_-^{(k)}\gamma_i^{(k)}\right)\right\}$
- to the majority ions	$\tau_e^{(k+1)}\left(\alpha_M^{(k)} + \tau_i^{(k)}R_-^{(k)}\alpha_M^{(k)}\right)$
- reflected	$\tau_e^{(k+1)}\tau_i^{(k)}R_-^{(k)}\tau_i^{(k)}$
- transmitted	$\tau_e^{(k+1)}\tau_i^{(k)}T_-^{(k)}$

3.2 – Evaluation of the total power balance. A simple algorithm allows to estimate the total power balance. The plasma cross–section being divided into N regions by the resonance layers, two arrays $P_+(j)$ and $P_-(j)$ are foreseen to contain, for each region, the power *which has not yet been absorbed* flowing to the left and to the right, respectively. Assuming for example that the antenna is on the outer side of the tokamak, $P_+(1)$ is initialised to $P(n_\varphi)$ and all other elements of $P_+(j)$ and $P_-(j)$ are initialised to zero. The scattering scenario appropriate to the first resonance layer is then applied: the absorbed power is attributed to the various species, the transmitted power is attributed to $P_+(2)$, and the reflected power to $P_-(1)$; finally, $P_+(1)$ is reset to zero. The same procedure can now be applied to the second region, $P_+(2)$ now playing the role of incident flux, and so on, until the inner wall is reached with an incident power flux $P_+(N)$. The fractional power deposited in the plasma up to this point is by definition the *single transit efficiency.*

Reflection at the wall is next implemented by setting $P_-(N) = (1 - \alpha_w^i)\,P_+(N)$ followed by $P_+(N) = 0$. The whole procedure is then repeaed proceding toward the outside, picking up the fluxes $P_-(k)$ from the previous transit, and so on, until absorption is complete.

It will be noted that the procedure just described is not strictly rigorous, since it assumes that the power fluxes of successive transits are additive, thereby excluding constructive or destructive interference effects occurring near resonance layers. This is at least partly justified by the fact that such effects, if present, must vary rapidly with the vertical position, since the real geometry is far from being plane–layered. Thus even if locally inaccurate, the obtained estimates should be correct at least in an averaged sense.

3.3 – Power deposition profiles. The evaluation of power deposition profiles is optional. For the purpose, magnetic surfaces are assumed to be similar ellipses of aspect ratio b/a, and are labeled by a variable ψ increasing from 0 on the magnetic axis to 1 at the plasma edge; a mesh in ψ is taken with uniform step $\Delta\psi$.

The power deposited on the electrons by TTMP and Landau damping is distributed at each point of the radial mesh proportionally to the local value of γ_e (Eq. (20)). The power absorbed by cyclotron damping and by both species through mode conversion is distributed assuming that the wave illuminates each resonance surface uniformly within a "beam" of height $2h$, where h might be anything between the half–length of the antenna and the vertical plasma radius b, and is to be specified by the user. The inner and outer magnetic surfaces cut by the illuminated region are

$$\psi_1 = \frac{|X_o - R_a|}{a} \qquad \psi_2 = \left(\frac{(X_o - R_a)^2}{a^2} + \frac{h^2}{b^2} \right)^{1/2} \tag{32}$$

where $X_o - R_a$ is the distance of the resonance layer from the magnetic axis. To obtain the density of power absorbed between ψ and $\psi + \Delta\psi$, $\psi_1 \le \psi \le \psi_2$, the total power deposited is weighted with $nT/(\Delta V \,|\sin\Theta|)$, where

$$\Delta V = (2\pi R_a) \cdot (\pi ab) \cdot \psi \, \Delta\psi \tag{33}$$

is a crude estimate of the volume of the shell $\Delta\psi$, and

$$\sin\Theta = \frac{b(\psi - \psi_1)}{\sqrt{a^2\psi^2 + b^2(\psi - \psi_1)^2}} \tag{34}$$

takes roughly into account the inclination of the magnetic surface with respect to the vertical (to avoid divergences, $\psi - \psi_1$ is limited from below to $\Delta\psi$). The factor nT takes into account that all damping mechanisms are proportional to the local plasma pressure.

These rather crude estimates could be improved for example by taking into account the Doppler broadening of cyclotron resonances, and by a better description of the real plasma geometry. It is however doubtful whether more accurate results would thereby be obtained. Indeed, the largest source of uncertainty is the vertical distribution of the power flux density incident on resonance layers, for which a reliable guess is hardly available. On the other hand both the physics of h.f. waves damping and the geometry of magnetic surfaces strongly wheight the power deposition towards the equatorial plane: as a consequence, the profiles obtained are only moderately sensitive to the assumptions made here.

4. – Examples and comparisons with other codes.

In this section we present a few examples to illustrate the use of the ICEVAL routine. They were run in the first place to compare the predictions of ICEVAL with those of a full–wave code, in order to check the validity of the assumptions made in the elementary model described above. For the purpose we have used the code FELICE [2], which combines the solution of the finite Larmor radius wave equations in a plane–stratified plasma with a fully self–consistent 3-dim. treatment of the antenna. It turns out that agreement is remarkably good, if allowance is made of the limitations of the elementary model (and of FELICE as well). Even in cases where agreement is not complete, the comparison helps in interpreting the results of both codes, and improves the understanding of the physics of ICR heating.

We also show how ICEVAL can be used to investigate the effects of quasilinear minority heating on the first pass absorption and on the global power balance. No easily performed test of these results is available, as discussed below: in this case the simple model of section (2.5) opens the possibility of exploring, qualitatively but with very little effort, the interesting non–linear interplay between power level and absorption efficiency.

Similarly, accurate power deposition profiles can be obtained only from a full–wave code in toroidal geometry. The profiles produced by ICEVAL must be regarded as qualitative only; they are nevertheless a reasonable guess for the interpretation of experiments and as input to transport codes.

4.1 – Antenna spectrum. Typical fast wave spectra extend to $n_{\varphi\,MAX} \simeq 30$ to 50, depending on the frequency and antenna configuration. The width of the spectrum explored by ICEVAL can be specified by the user, or can be estimated by the code from the exponential evanescence factor described in section 2.1. The distance d_{ap} between the Faraday screen and the plasma edge can be chosen to influence the spectral width: the best results are usually obtained by taking d_{ap} to be the distance from the antenna conductor(s) to the separatrix or limiter radius, i.e. by considering the scrape–off as a vacuum layer. It is also possible to specify wether all toroidal modes should be considered, or only a sample (up to one mode in 5; the latter option is taken automatically if the arrays over toroidal modes are underdimensioned for the specified spectral width). It is however preferable to scan all modes, to cover adequately the critical region $n_{\parallel}^2 = O(1)$; this requires the dimensions of the corresponding arrays to be at least $2n_{\varphi\,MAX} + 1$.

The spectra described by Eq. (1) are always smooth, and have the form which would be predicted by full–wave codes in the limit of complete absorption in a single transit (this situation can be simulated in FELICE by imposing outward radiation conditions at some distance from the antenna). By contrast, the spectra obtained by full–wave codes when integrating over the entire plasma cross–section are mostly spiky, because of the preferred excitation of cavity eigenmodes, particularly when the single–transit absorption is weak. Two examples are shown in Fig. 1 for typical monopole and dipole antennas ($w_A = 18$ cm, $g_A = 16$ cm in the dipole case; $f = 45$ Mhz). The spectra shown for comparison are obtained with the FELICE code for a deuterium plasma with hydrogen minority (cfr. the next paragraph). Eigenmodes are clearly visible in the case of a pure D^+ plasma, in which the single pass absorption is only about 20%. With 5 % H^+ minority absorption is much stronger, and eigenmodes are fairly suppressed also in the FELICE simulation. In situations in which FELICE does not predict eigenmodes (particularly the dipole case with outward radiation conditions; in the monopole configuration a surface wave with $n_\varphi = 0$ is strongly excited even in the absence of global eigenmodes) agreement is excellent.

The impossibility of simulating eigenmodes excitation with ICEVAL must be taken into account when comparing the predictions of this subroutine with those of a full–wave code. We would like to stress however that this is not necessarily a limitation of ICEVAL. Indeed, it is well–known that full-wave codes in plane–stratified geometry tend to overestimate the excitation of cavity eigenmodes, both with respect to the experimental evidence and to the results of fully toroidal codes [3].

4.2 – Power balance in the linear approximation. The simplest check of the absorption model described in sections 2 and 3 consists in comparing the global power balances in the linear approximation from ICEVAL and FELICE as a function of the minority concentration in a few ICR heating scenarios. Here we present the case of Hydrogen minority in a Deuterium plasma for parameters typical of the ASDEX Upgrade ICR heating experiment. Two other interesting scenarios, namely He_3 minority in Hydrogen or Deuterium, will be discussed in a separate report [7].

The results for the case of H^+ in Deuterium are summarised in figs. 2. The plasma parameters were chosen to be: central density $n_e = 8.\ 10^{13}$ cm^{-3}; central temperatures $T_e = T_D = 2$ keV, $T_D = 3.2$ keV; magnetic field on axis 3 Tesla, applied frequency 45 Mhz. The plasma radius is 50 cm and the major radius 165 cm.

With default values taken for all adjustable parameters, the initial steepness of $P(H)$

(the fraction of power absorbed by the minority) at low concentration is accurately reproduced by ICEVAL; at higher concentrations the value of $P(H)$ is also in very good agreement if averaged over the dip predicted by FELICE around $n_H/n_e \simeq 0.12$. The fraction deposited in the electrons on the other hand is overestimated by 10 to 15% at low concentration, and underestimated by the about same amount at large concentrations, again averaging over the peak around $n_H/n_e \simeq 0.12$. For a fair comparison of the results for the electrons however it is necessary consider the differences between the two codes in some more detail. FELICE gives separate information on the amount of power which is mode–converted to ion Bernstein waves (IBW); in ICEVAL this power is immediately attributed to the electrons. If $P(IBW)$, which is a rapidly decreasing function of n_H/n_e, is added to $P(e)$ in the FELICE case, the discrepancy at low concentration disappears. A detailed analysis of the power deposition profiles from FELICE shows that a non negligible amount of power is dissipated collisionally on the electrons very close to the plasma edge, more precisely in the h.f. skin layer (of thickness $\sim c/\omega_{pe}$) in which the parallel electric field adjusts from its value in vacuum to its much smaller value in the plasma. The effect is stronger when the single pass absorption is weak, since in this case all fields in the plasma are larger, and is of course not taken into account in ICEVAL. To simulate it, we have assumed that 0.25 % of the incident power is lost at each reflection from the outer wall. If the resulting total losses (the curve marked "wall" in fig. 2 b) are attributed to the electrons, agreement becomes as good as for the minority at all concentration.

The dip in $P(H)$ and the corresponding peak in $P(e)$ in the FELICE results at intermediate concentrations are due to eigenmodes. Above $n_H/n_e \simeq 0.08$ the layer between the ion–ion cutoff and resonance in which the compressional wave is evanescent becomes optically thick ($\eta \gtrsim 1$), and a standing wave can accomodate between the cutoff and the outer wall. Such a localised eigenmode appears first with low $n_\parallel$ when $n_H/n_e \simeq 0.10$, and moves toward larger $n_\parallel$ as the concentration increases further. Its quality factor is particularly large at low $n_\parallel$, where the only damping mechanism available is collisional absorption by the electrons. As its parallel index increases, the resonant mode becomes subject to damping by the ions as well, and $P(H)$ increases again somewhat.

That ICEVAL cannot reproduce this behaviour is not astonishing. One should note however that in toroidal geometry even a mode with toroidal wavenumber $n_\varphi = 0$ has a relatively broad spectrum of $k_\parallel$ in the center of the plasma due to strong coupling between poloidal components [3], and is therefore subject to appreciable ion damping. This is likely to reduce the quality factor of eigenmodes, so that the predictions of

ICEVAL might actually be closer to reality than those of FELICE.

4.3 – Quasilinear minority heating. Once convinced of the reliability of ICEVAL, its great flexibility makes it tempting to use it to explore a wider parameter range than reasonably feasible with the much heavier full–wave code. Here we have limited these explorations to the investigation of the effects of quasilinear minority heating on the first pass absorption and on the global power balance. To obtain comparable results with FELICE one should couple this code iteratively with a Fokker-Planck solver such as FPSOLV [8]: in an iterative procedure similar to the one described in section 2.5, FELICE provides the heating rate to be used in the quasilinear diffusion coefficient in FPSOLV, and FPSOLV provides the ion distribution functions to be used to evaluate IC absorption in FELICE. This has been done in the case of pure second harmonic heating [9], for which approximate analytic solutions of the Fokker-Planck equation are not available. The systematic use of the two codes in this way however is a rather slow procedure. Moreover, in estimating the quasilinear velocity diffusion coefficient to be used in FPSOLV one encounters the same uncertainty in the definition of the effective heated volume ΔV_{eff} which has been pointed out above in the case of ICEVAL (cfr. Eq. (27)). A convincing check of the predictions of ICEVAL would therefore require a fully toroidal wave code, coupled with the solution of the Fokker–Planck equation at a number of magnetic surfaces: this is not yet feasible (it is of course possible, however, to prove that the predictions of the Stix model agree reasonably well with the numerical solutions of the Fokker–Planck equation for a *given* heating rate, provided that heating itself is not too fast).

Fig. 3 shows the effective temperature of the H^+ ions and the first pass absorption versus minority concentration at different values of the total launched power; fig. 4 shows the fraction of power going to H^+ and to the electrons. The plasma and h.f. parameters are the same as in the previous examples. The physics behind these results is very simple: increasing the minority temperature increases cyclotron damping by the minority and the first pass absorption, while less power remains available for direct electron heating. The strength of the effect however is a strongly non–linear function of the applied power. Moreover, for a given power, it decreases rapidly with increasing concentration, not only because the available power per minority ion is inversely proportional to their number, but also because the field at the cyclotron resonance decreases as screening of E_+ by the resonant ions increases . The usefulness of a simple but self–consistent model to evaluate the final result is obvious. It would of course also be desirable to check quantitatively the predictions of ICEVAL with a more complete model.

4.4 – Spectral power balance and power deposition profiles. Additional information can be obtained from ICEVAL about the spectral repartition of the power balance. An example is shown in Fig. 5 for the case of 5 % Hydrogen in Deuterium (dipole antenna, other parameters as before). The amount of power to each species is proportional by the corresponding area. As expected, electron damping is shifted somewhat towards larger n_φ values ($n_\varphi = 10$ corresponds to $n_\parallel = 6.426$) with respect to cyclotron damping. In FELICE this effect is somewhat masked by collisional damping in the h.f. skin layer, which is stronger for low $n_\parallel$ modes. The power lost to the wall in the result of ICEVAL, and the power mode–transformed to Bernstein waves in those of FELICE, are omitted in fig. 5.

Power deposition profiles evaluated according to the model of section 3.3 are shown in fig. 6 for the same case; the plasma cross-section was assumed elliptic, with $a = 50$ cm and $b = 80$ cm. As expected, the power deposition densities $W(\psi)$ are strongly peaked towards the plasma center, mainly because of the decreasing specific volume of magnetic surfaces near the magnetic axis. Nevertheless, even the products $W(\psi) \cdot r$ have a marked maximum at the magnetic surface which is just tangent to the resonance (in this case, about 3 cm away from the axis). This is due partly to the geometric $(\sin \Theta)^{-1}$ effect, and partly to the assumed proportionality of the absorption efficiency to the plasma pressure nT. Because of these effects, the shape of the profiles is relatively insensitive to all other assumptions and to the particular heating scenario.

References.

[1] Brambilla M., Report IPP 5/3, February 1987.

[2] Brambilla M., Comp. Phys. Rep. **4** (1986) p. 71, and references therein.

[3] Brambilla M., Plasma Phys. Contr. Fusion **31** (1989) 723, and references therein.

[4] Brambilla M., Kruecken T., Nucl. Fusion **28** (1988) 1813, and references therein.

[5] Budden K.G., *Radio waves in the Ionosphere*, Cambridge Univ. Press 1955, Ch. 21.

[6] Stix T.H.,Nucl. Fusion **15** (1975) 737.

[7] M. Brambilla, J.-M. Noterdaeme, in preparation.

[8] C. Hoffman, Doctorate Thesis, Garching 1992.

[9] M. Brambilla, C. Hoffman, to be published.

APPENDIX

The subroutine ICEVAL is called as

CALL ICEVAL(INITCH,IANTSP,ICYRES,IPWRAD)

The following is a list of the arguments and common variables of ICEVAL.

```
C
C ============================================================
C
C  ARGUMENTS:
C
C    the arguments are input parameters which control
C    the execution of optional sections of ICEVAL:
C
C    To have an operation performed (initialisation, spectre, etc.,
C    the user should set the corresponding parameter to 1;
C    the parameter is automatically reset to 0 by ICEVAL, so that
C    the operationis not repeated unless explicitly required
C    again by the user.
C
C  INITCH = 1 :  print the run parameters.
C  IANTSP = 1 :  evaluate the antenna power spectre P(nz);
C                required only at the first call.
C  ICYRES = 1 :  evaluate the position of ion cyclotron resonances.
C                Required at the first call, then only if
C                the magnetic field BZERO has changed.
C  IPWRAD = 0 :  power deposition profiles skipped.
C         = 1 :  Power deposition profiles evaluated.
C
C  NOTE:  IANTSP and ICYRES must be set to 1 at the first
C         call of the subroutine ICEVAL, otherwise
C         data on the launched spectre and the position of
C         IC resonances will not be available.
C         It is assumed that variables interne to the ICEVAL
C         subroutine are 'saved' between successive calls.
C
C ============================================================
C
```

```
C
C ================================================================
C
C  EXTERNALS:
C
C   The following profile functions should be available
C   (a set comes the MAIN program which is supplied to run
C   ICEVAL as a stand-alone package):
C
C  PRONE(PSI) should give the density profile
C  PROTE(PSI) should give the electron temperature profile
C  PROTI(PSI) should give the ion temperature profile
C         (all species assumed to have the same T profile)
C
C         where PSI should label magnetic surfaces linearly in r/a
C         from 0 (magnetic axis) to 1 (plasma edge).
C         The normalisation and units used are irrelevant:
C         the central density DENC and temperatures
C         TEMPEC, TEMPIC(i) have to be specified separately
C         (see list of input COMMON variables).
C
C  NOTE:  ICEVAL calls no external routines other than those
C         providing density and temperature profiles.
C
C ================================================================
C
C  PARAMETERs
C
C   The following parameters can be modified by the user
C   if the standard options are inadequate for some application:
C
C  NSP    (integer) dimension of arrays over the ion species
C  NZDIM  (integer) dimension of arrays over the n// spectre
C  NPSI   (integer) dimension of arrays for power deposition profiles
C
C ================================================================
C
```

```
C
C ===============================================================
C
C  Input COMMON variables
C
C   The following variables are to be initialised by the user
C   calling the subroutine ICEVAL:
C
C      r = real;        i = integer
C      s = scalar;      a = array
C
C  Plasma parameters
C  ================
C  RTORUS (r,s)   toroidal radius (to the mid-point, cm)
C  RPLASM (r,s)   plasma radius in the equatorial plane (cm)
C  DMAXIS (r,s)   displacement of the magnetic axis (cm)
C  ELLIPT (r,s)   ellipticity (b/a) of the plasma cross-section
C  BZERO  (r,s)   magnetic field at the mid-point (tesla)
C  DENC   (r,s)   electron density on the magnetic axis (cm-3)
C  TEMPEC (r,s)   electron temperature on the magnetic axis (keV)
C  NSPEC  (i,s)   number of ion species (must not exceed NSP
C  MAINSP (i,s)   majority species (preferably without fundam.
C                   cycl.  resonance within the plasma)
C  ATM    (r,a)   ion mass (atomic units)
C  AZI    (r,a)   ion charge (atomic units)
C  ACONC  (r,a)   number density concentration of each species
C                   (can be omitted for the majority species)
C  TEMPIC (r,a)   ion temperature on the magnetic axis (keV)
C
```

```
C
C  H.F. and antenna parameters
C  ==========================
C  FREQCY (r,s)   frequency (hz)
C  POWER  (r,s)   total coupled power (MW)
C  JPOLE  (i,s)   type of antenna:
C       JPOLE = 1 - Dipole antenna (1 conductor)
C       JPOLE = 2 - Quadrupole antenna (2 conductors)
C  WGAP   (r,s)   distance between conductors (cm)
C                   (ignored if JPOLE=1)
C  EPHASE (r,s)   phase between conductors (degs)
C                   (ignored if JPOLE=1)
C  DISTAP (r,s)   distance antenna-plasma (cm)
C                   (increasing DISTAP makes the spectre narrower)
C  HEIGHT (r,s)   poloidal half-length of the antenna
C  WIDTH  (r,s)   toroidal width of each conductor (cm)
C  ISIDE  (i,s)   location of the antenna:
C       ISIDE =  1 - to the outside;
C       ISIDE = -1 - to the inside.
C  AWALLE (r,s)   fractional absorption at refl.  from the outer wall
C  AWALLI (r,s)   fractional absorption at refl.  from the inner wall
C  NPHMAX (i,s)   maximum toroidal number in the antenna spectre
C  JUMPHI (i,s)   step in the toroidal wavenumber
C                   (automatically increased if 2*(NPHMAX/JUMPHI)+1
C                   exceeds NZDIM; max.  accepted value JUMPHI=5)
C  ISTIX  (i,s)   Quasilinear correction to the minority temperature:
C       ISTIX  = 0 :  Iteration over Stix correction skipped
C       ISTIX  = 1 :  Iteration over Stix correction made
C
C  Control of the printed output:
C  ==============================
C  IOUTPR = 0 :  print reduced to a minimum.
C         = 1 :  print intermediate results.
C         = 2 :  print plasma parameters, details of resonances, etc.
C               (for use as an autonomous package only)
C
```

```
C
C         NOTE: no plot is executed by ICEVAL.
C               The MAIN program supplied to run ICEVAL
C               as a stand-alone package has plotting facilities,
C               which hoewever are installation dependent.
C
C  Tuning parameters:
C  ==================
C  QYFACT (r,s)   numerical factor in the surface admittance
C                   Re(Y) = 1 + QYFACT*(0.1*Nz**2/(1.+0.1*nz**2))
C  ANGLCO (r,s)   Geometrical factor in the optical thickness
C                   of evanescent layers:
C       ANGLCO = 1.  - wavefronts perpendicular to the layer.
C       ANGLCO > 1.  - wavefronts oblique to the layer.
C  QFDOPL (r,s)   Doppler effect on mode conversion.
C  QFCYCL (r,s)   numerical factor in the evaluation of absorption
C                   at fundamental cyclotron resonances.
C  QFHARM (r,s)   numerical factor in the evaluation of absorption
C                   at first cyclotron harmonics.
C  QFQLIN (r,s)   Correction to the 'crude' Stix formulas
C                   for the quasilinear effects on minority heating
C                   (QFQLIN = 0.  is equivalent to ISTIX = 0)
C  QFCOLL (r.s)   numerical factor in the collisional absorption.
C  QFTTMP (r,s)   Correction to the electron TTMP (and ELD) absorption
C
C ============================================================
C
C  Output COMMON variables
C
C   The following variables constitute the output of ICEVAL:
C
C         Spectral power distributions
C         ============================
C  NUMPHI      (i,a)   number of partial waves in the spectre
C  ANZ(nz)     (r,a)   parallel index of partial wave nz
C  PWCPL(nz)   (r,a)   fraction of power coupled to partial wave nz
C  PWE1(nz)    (r,a)   fraction of power absorbed by the electron
C                        for partial wave nz (first transit)
```

```
C  PWE(nz)     (r,a)   fraction of power absorbed by the electron
C                       for partial wave nz (total)
C  PWI1(i,nz) (r,a)   fraction of power absorbed by ions species i
C                       for partial wave nz (first transit)
C  PWI(i,nz)  (r,a)   fraction of power absorbed by ions species i
C                       for partial wave nz (total)
C
C        Power deposition profiles
C        =========================
C  PSI(n)      (r,a)   points in the profies (equidistant,
C      from PSI = 0 on the magnetic axis
C      to   PSI = 1 at the plasma edge
C  PSPWE(n)    (r,a)   power absorption profile for the electrons (W/cm3)
C  PSPWI(i,n) (r,a)   power absorption profile for the ions i    (W/cm3)
C
C        First transit energy balance
C        ============================
C  PFRST       (r,s)   fraction of power absorbed
C  PFRSTE      (r,s)   fraction of power absorbed by the electrons
C  PFRSTI(i)   (r,a)   fraction of power absorbed by ions i
C
C        Global energy balance
C        =====================
C  PTOTE       (r,a)   fraction of power absorbed by the electrons
C  PTOTI(i)    (r,a)   fraction of power absorbed by ions i
C  PWALLE      (r,s)   fraction of power to the outer wall
C  PWALLI      (r,s)   fraction of power to the inner wall
C  TEFF(i)     (r,a)   effective temperature of species i (Stix)
C
C ============================================================
```

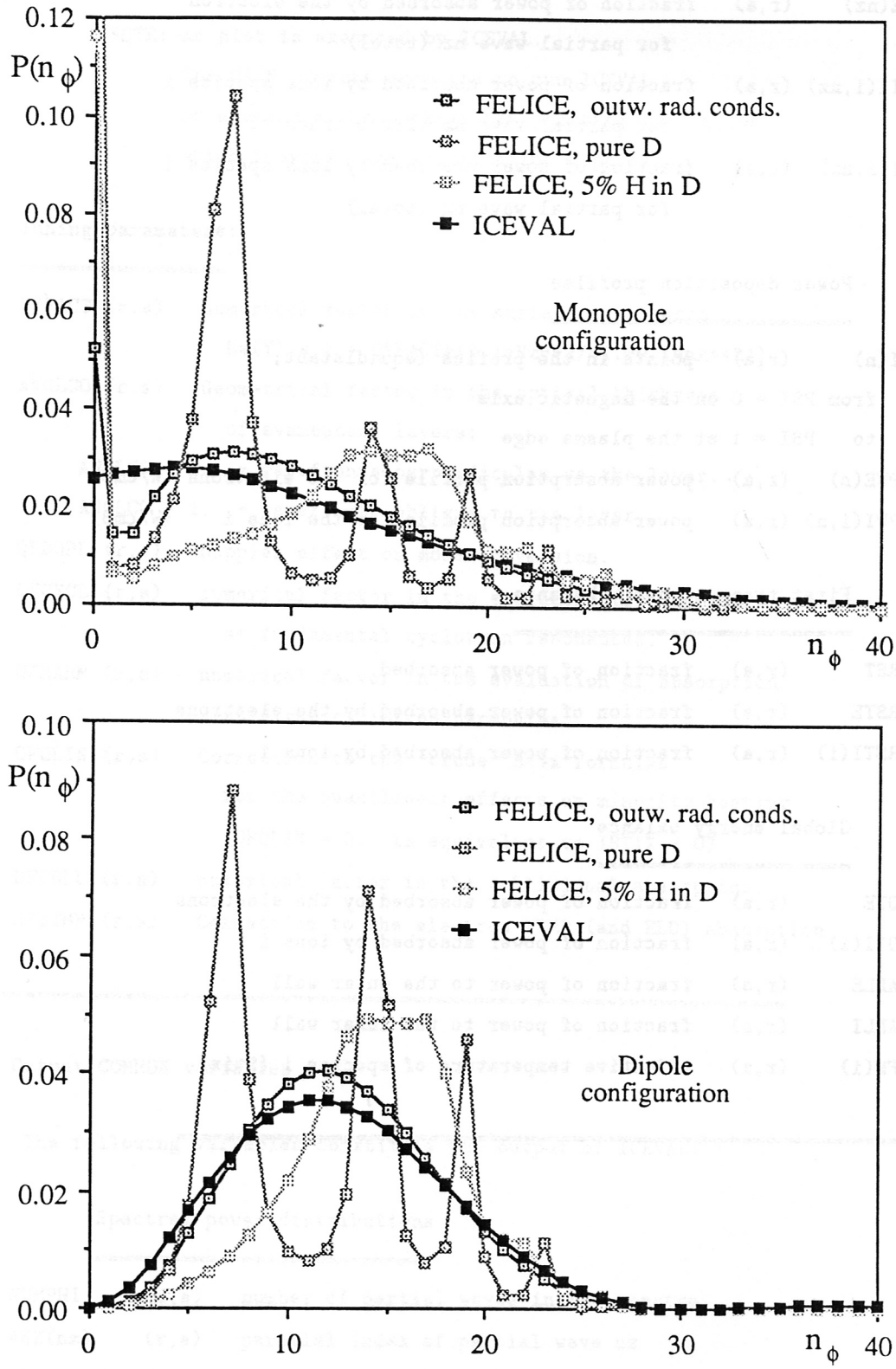

Fig. 1 - Power spectrum simulation. Comparison of the ICEVAL model with a few cases computed with the full-wave code FELICE.

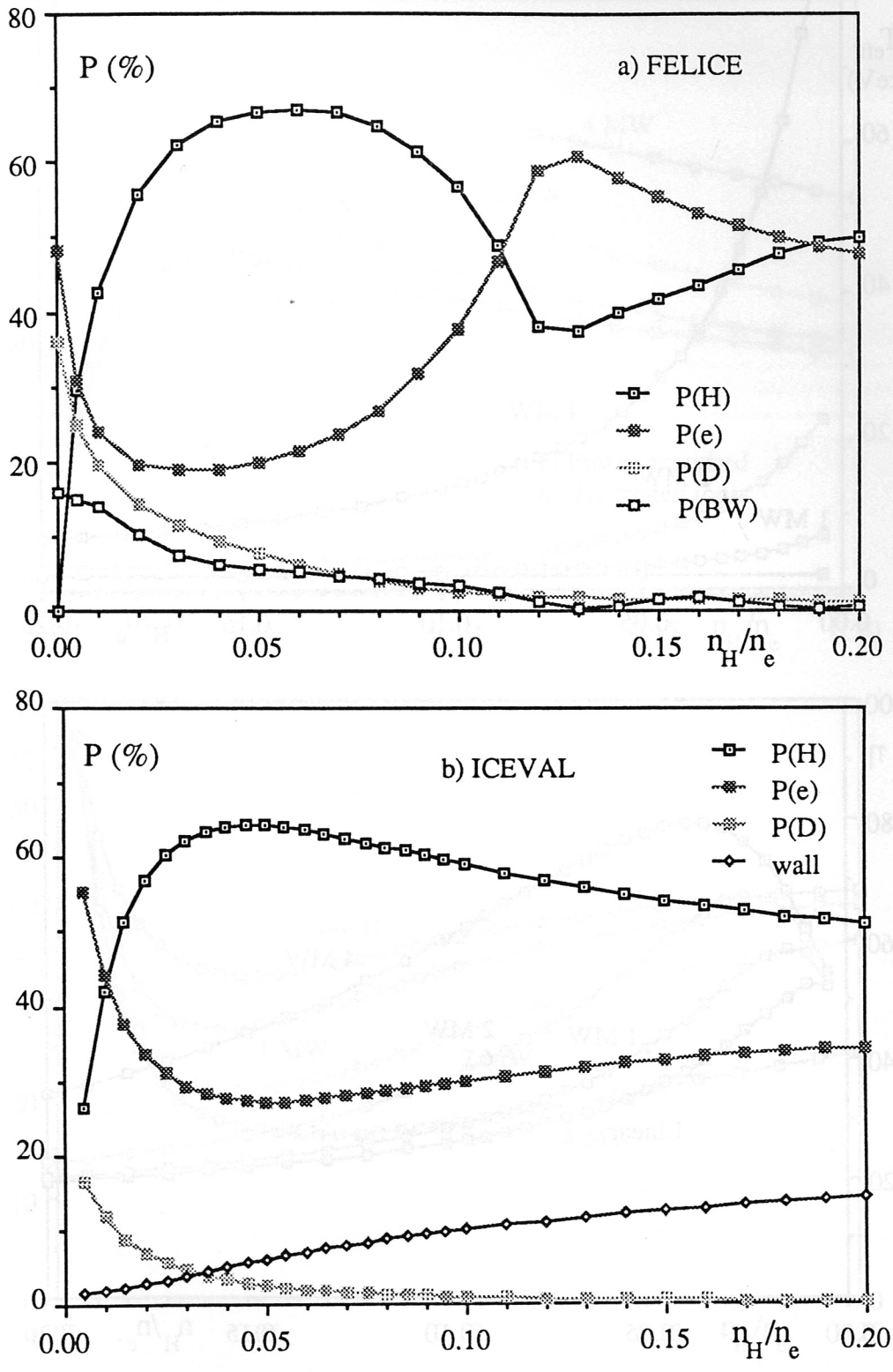

Fig. 2. - H minority in a D plasma (Asdex Upgrade plasma, dipole antenna) Comparison of the power balance from the full-wave code FELICE and from ICEVAL. Linear damping, $T_e = T_D = 2$ keV, $T_H = 3.2$ keV.

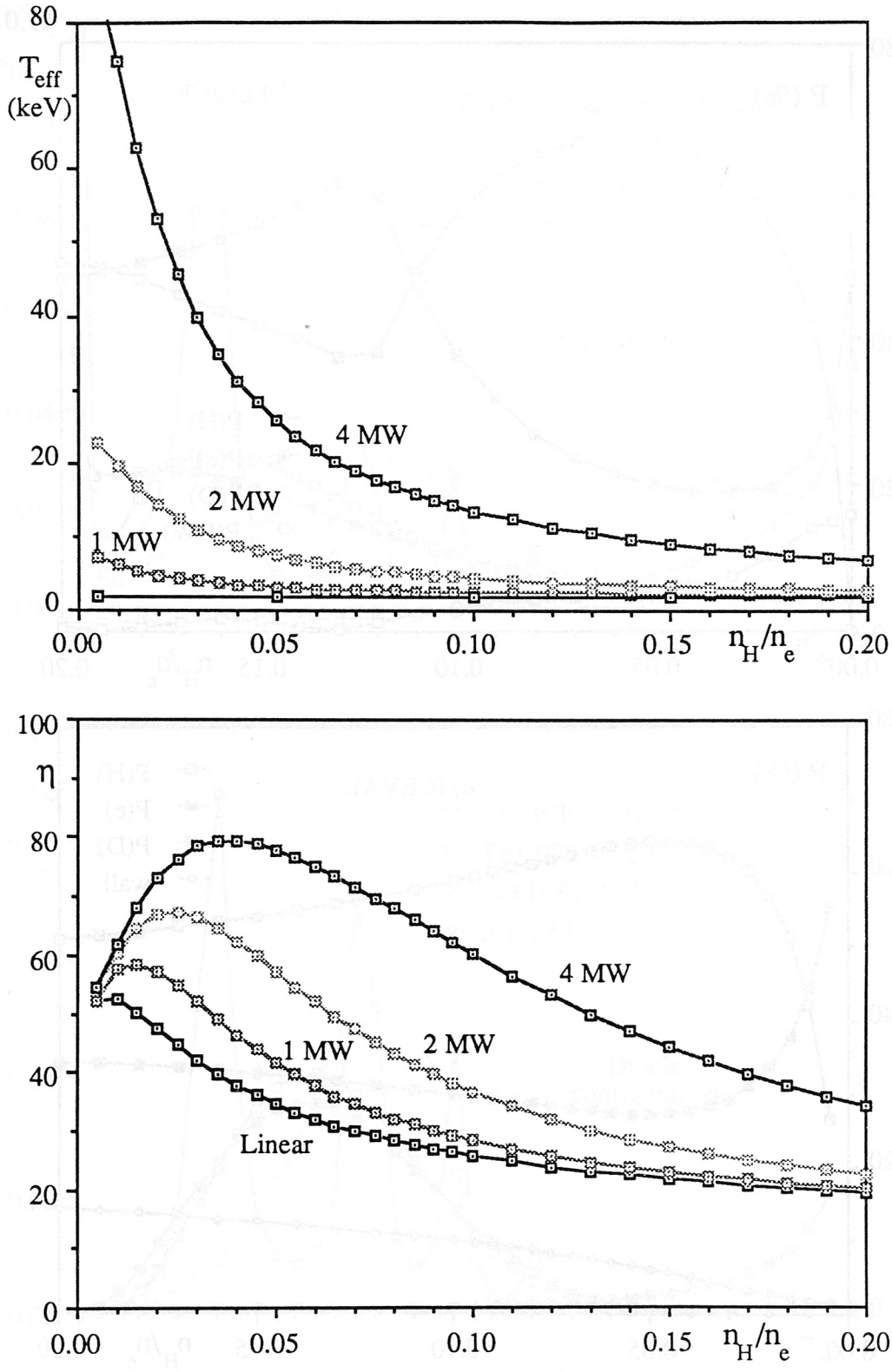

Fig. 3 - H minority in a D plasma (Asdex Upgrade, dipole antenna): Effect of quasilinear heating: a) effective temperature of the minority; b) first transit absorption versus applied power.

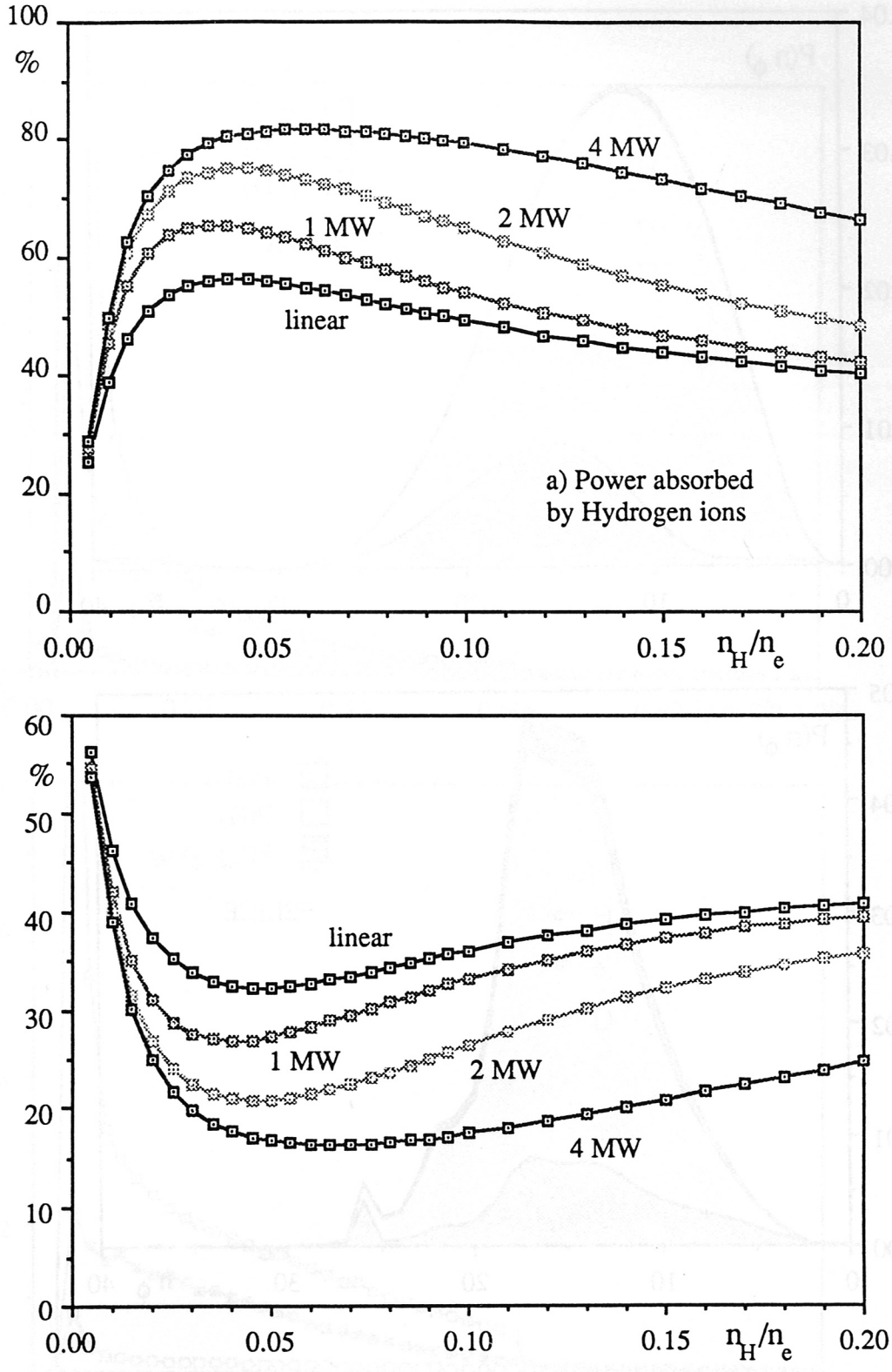

Fig. 4 - H minority in a D plasma (Asdex Upgrade, dipole antenna). Effect of quasilinear heating on the power balance: a) fraction absorbed by H; b) fraction absorbed by the electrons at various power levels.

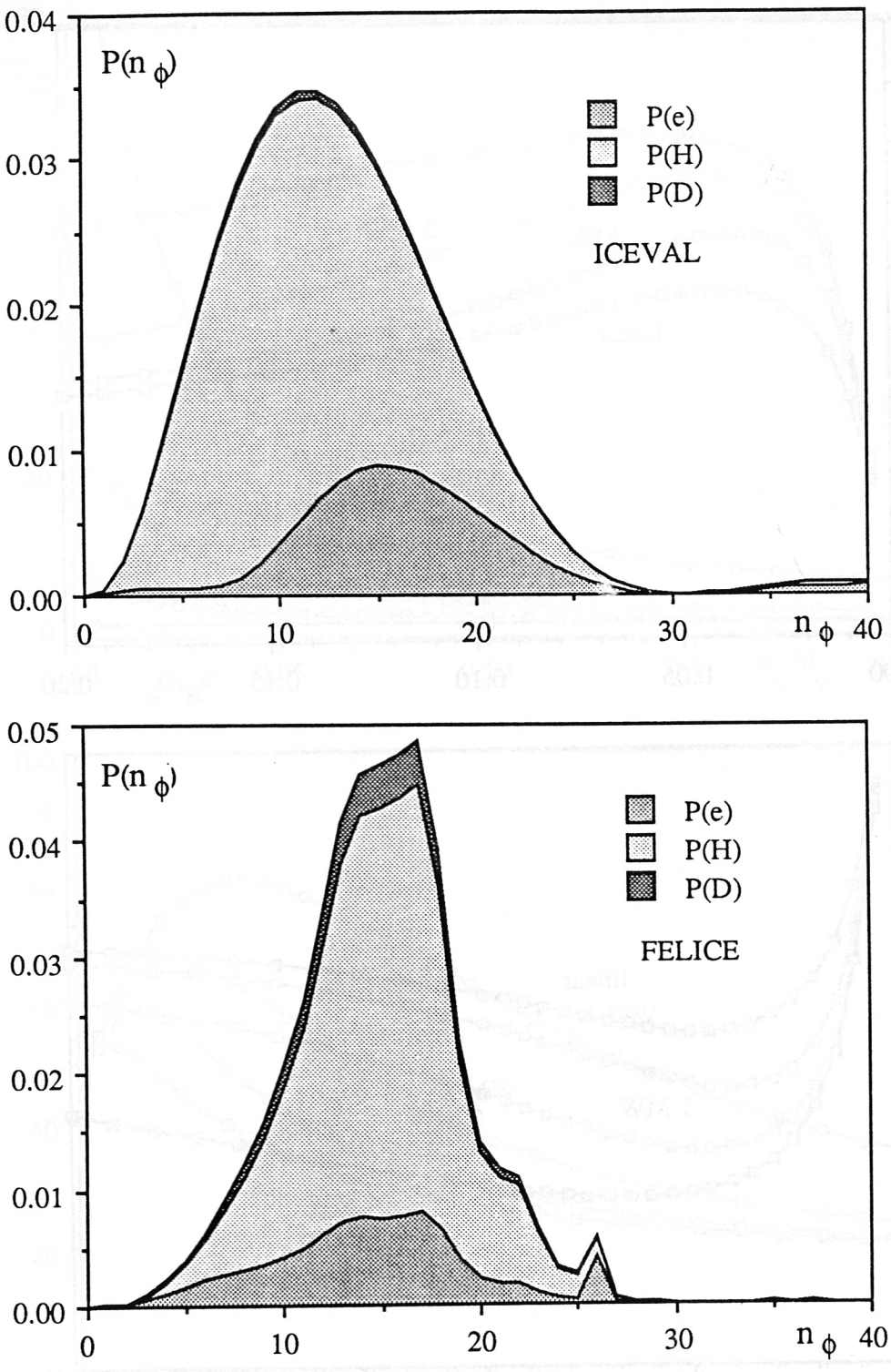

Fig. 5 - Spectral repartition of the absorbed power. 5% H in a D plasma, (Asdex Upgrade, dipole antenna).

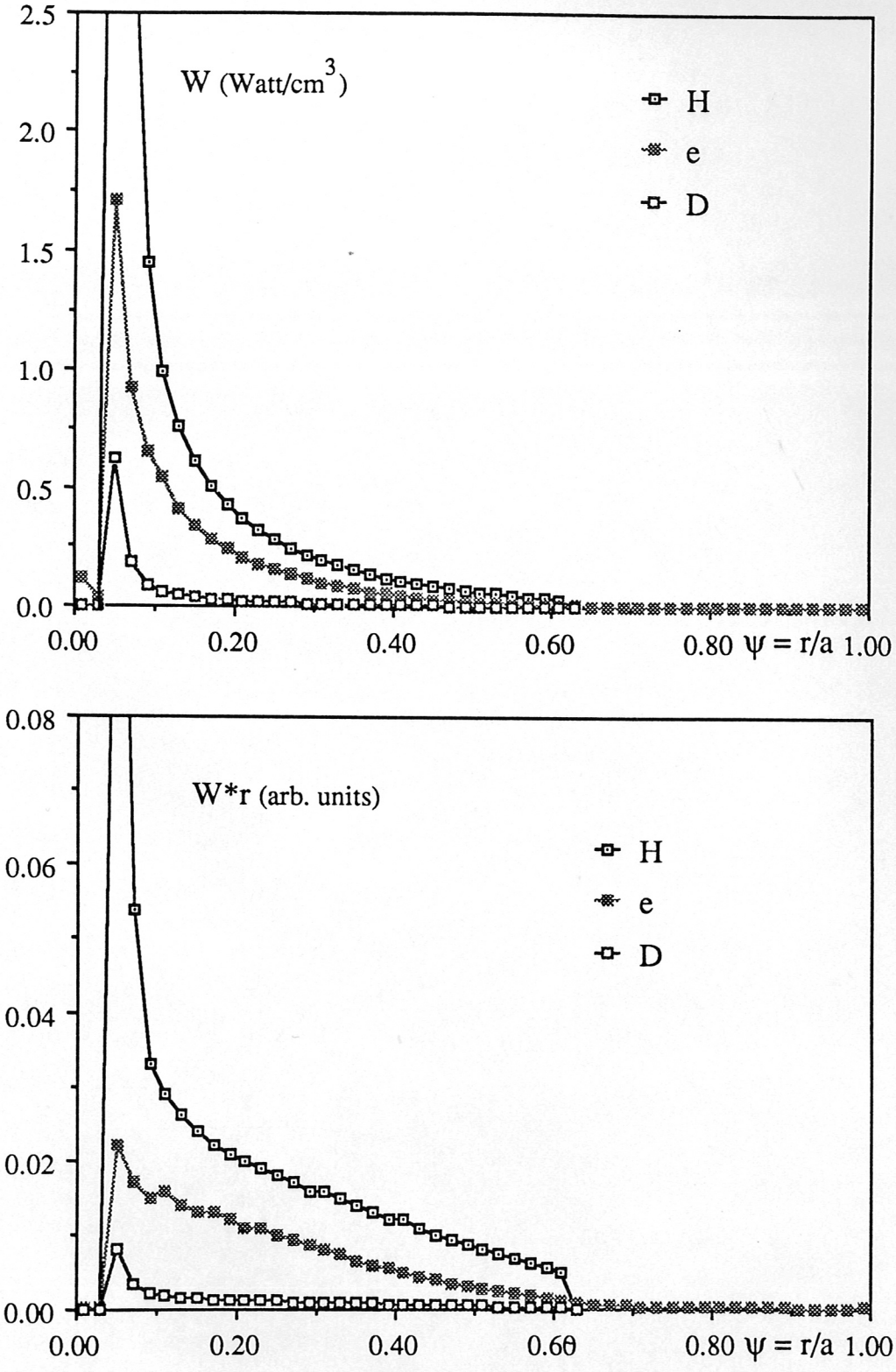

Fig. 6 - Power deposition profiles (5% Hydrogen in Deuterium, dipole antenna configuration, total power coupled 1 MW.